A dynamo model for the magnetic field of the weakly barred galaxy IC 4214

D. Moss,[1] P. Rautiainen[2] and H. Salo[2]

[1]*Mathematics Department, University of Manchester, Manchester M13 9PL*
[2]*Department of Physical Sciences, Astronomy Division, PL 333, University of Oulu, FIN 90571 Oulu, Finland*

ABSTRACT

IC 4214 is a weakly barred galaxy, the observed velocity field of which has been well modelled by a dynamical simulation. We take the velocity field from this simulation as being representative of that to be found in a class of barred spiral galaxies, and use it as input into a galactic dynamo model. The strong non-circular velocities are found to play an important role in determining the morphology of the magnetic field. The most conspicuous features are marked magnetic 'arms', steady in the frame corotating with the bar, and trailing from near the ends of the bar. They are generated by a mechanism associated with the corotation resonance. Near the centre of the galaxy, the magnetic field is approximately axisymmetric. The computed magnetic field structure has features similar to those of the fields observed in barred galaxies.

Key words: magnetic fields – MHD – galaxies: individual: IC 4214 – galaxies: kinematics and dynamics – galaxies: magnetic fields – galaxies: spiral.

1 INTRODUCTION

In the last decade or so, radio observations have revealed the gross structure of the large-scale magnetic fields present in a number of spiral galaxies (see, e.g., Beck et al. 1996 for a review and further references). A more recent, and exciting, development is that high-quality observations of barred spiral galaxies are now becoming available (Frick et al. 1998).

So far, most theoretical attention has been directed to explaining the magnetic fields present in 'normal' spiral galaxies. The crucial ingredients are a knowledge of the rotation curve and, in the context of mean-field dynamo theory, enough information about the properties of the ionized gas in order to be able to make an estimate of the alpha effect. Barred spiral galaxies differ in that large non-circular velocities ('streaming motions') are present. These are typically 50 km s^{-1}, or even larger, and will modify the magnetic field produced by any conventional dynamo process. For example, the magnetic Reynolds number $Rm = Ul/\eta \sim 50-150 \gg 1$, if $U = 50$ km s^{-1}, $l = 0.3-1$ kpc, and $\eta = 10^{26}$, where l is a length scale, U a typical velocity and η the effective magnetic diffusivity. Thus, a priori, good data for these non-circular motions are essential if magnetic field structures in barred spiral galaxies are to be modelled realistically. We note that streaming motions in non-barred grand-design galaxies are thought to be about 10 km s^{-1}, maybe less. Although ignored in conventional galactic dynamo models, Moss (1998) showed that even such relatively slow motions may be significant for the field structure.

In order to model dynamo processes and also to test the results, high-quality determinations of both the magnetic and velocity fields are needed. In particular, the global distribution of the velocity is required, including that in the central regions. In order to have a

reasonably high degree of confidence in the results, probably more than just the first couple of Fourier coefficients with respect to the azimuthal angle ϕ are needed. In general, observations do not provide enough information to satisfy all these requirements.

For these and other reasons, the modelling of magnetic field generation and structure in barred spiral galaxies has attracted relatively little theoretical attention. Chiba & Lesch (1994) studied the effect of non-circular gas motions on magnetic field generation and evolution. Their quite simplified model, making use of a local approximation to the induction equation, gives results that are hard to assess and compare with those of later authors. Brandenburg & Donner (in preparation) have investigated dynamo action in the galaxy M83, using velocity fields derived from simple density-wave theory considerations. Moss et al. (1998a) studied magnetic field evolution in a generic, non-steady, barred spiral galaxy model. Otmianowska-Mazur & Chiba (1995) have also investigated some aspects of the problem, although they did not model a complete dynamo process, and their fields thus could not be expected to be maintained over time intervals of Gyr length. Otmianowska-Mazur et al. (1997) used a velocity field derived from *N*-body simulations of barred galaxies, but again did not include a dynamo term in their induction equation, so their solutions also inevitably decay.

In this paper, we study the barred spiral galaxy IC 4214. This galaxy is a reasonably typical weakly barred spiral galaxy, with a well-determined velocity field (Buta et al. 1999). Simulations by Salo et al. (1999) employ a rigidly rotating bar potential, derived from a near-IR image (Buta et al. 1999). These reproduce the observed velocity field very satisfactorily and, we thus assume, provide a global determination of the velocity field (see Section 2). The main assumption of Salo et al., namely that the bar structure and pattern speed are steady over intervals of several Gyr, is

supported by the presence of an outer ring, a structure with a formation time of several Gyr (Combes 1996). We use the gas velocity field from this simulation as input into a dynamo calculation, in a manner similar to that described by Moss et al. (1998a). As mentioned above, that study differs in that that system did not settle to even an approximately steady state (in a rotating frame), and the velocity and so the magnetic fields were intrinsically unsteady. Another difference is that the dynamical model used here was a strong *N*-body bar. As in the majority of the calculations reported in that paper, we use here a two-dimensional simulation of the velocity field and a two-dimensional version of the dynamo code. These are outlined in Sections 2 and 3 respectively.

Although we have taken a model of a specific galaxy, we believe that the general features of the velocity field and associated magnetic field are likely to be representative of those in at least a subclass of barred spiral galaxies. We also note here that we assume that the production of poloidal magnetic field from toroidal, essential to maintain a large-scale magnetic field against decay, is brought about by the mean-field alpha effect. Whilst recognizing that this issue is the subject of some controversy (see, e.g., the discussion in Beck et al. 1996), we believe that it is plausible that it, or a similar process, operates (e.g. Parker 1992; Moss et al. 1998a, 1999). Nevertheless, the main point of this paper, the effects of the non-circular velocities, is expected to be independent of the details of the dynamo process.

2   THE DYNAMICAL SIMULATION

Ringed galaxies form a common subclass of barred galaxies. Their general properties have been modelled by various gas dynamical simulations using analytical or numerical potentials (Schwarz 1981; Combes & Gerin 1985; Byrd et al. 1994). These simulations have shown that rings and pseudorings are related to bar-induced resonances: outer rings to the outer Lindblad resonance, nuclear rings to the inner Lindblad resonance and inner rings probably to the inner 4/1 resonance. This interpretation is supported by observations (Buta 1995), and provides a powerful method for the determination of some basic parameters such as the bar pattern speed.

A step forward from these general studies is to model individual galaxies, preferably both their morphology and their kinematics. Many barred galaxies have been modelled (see e.g. Hunter et al. 1988; Lindblad, Lindblad & Athannasoula 1996) but few of those are clearly ringed.

We have constructed a dynamical model of IC 4214 (Salo et al. 1999), a weakly barred galaxy possessing all three types of resonance rings, by using the near-IR *H*-band image (Buta et al. 1999) to construct the potential. After removal of the bulge and deprojection, the gravitational potential is calculated using the Fourier components of the surface brightness distribution. The axisymmetric part is obtained from the $m = 0$ component and the non-axisymmetric part (bar and spiral arms) from $m = 2, 4, 6, 8$ and 10 components, each assumed to have the same pattern speed. The effect of the disc thickness is taken into account by a gravitational softening parameter, chosen so that the ratio of vertical to exponential scalelengths is about 1/6.

The evolution of the gas component was simulated by using 20 000 inelastically colliding test particles (Salo 1991). To obtain more velocity points, for determination of a smooth Eulerian velocity field for the dynamo calculations, data from 11 time-steps (corresponding to the same points in the rotating frame) were combined. The self-gravitation of the gas component was neglected.

The model parameters, e.g. bar amplitude and pattern speed, were fine-tuned by comparing both the morphology and the velocity fields with the observations. In this study we use two different models, one that fits well with the observations of IC 4214 (model I) and another that is quite different, for comparison (model II). Both models use the same non-axisymmetric basic potential but assume different pattern speeds. The pattern speed of model I is 37.3 km s^{-1} kpc^{-1} and it is 25 per cent higher in model II. Model II also lacks the bulge of model I, which is modelled as a Plummer sphere with scalelength of about 600 pc and mass 21.6 per cent of the disc mass. The latter causes the main difference between the models: model I has an inner Lindblad resonance while model II does not. In both models the halo contribution to the rotation curve is equal to that of the disc.

The evolution of the models shows the importance of the inner Lindblad resonance. Model I has a nuclear ring whereas Model II does not. Although this ring is rather distant from the radius predicted from the linear approximation (see e.g. Binney & Tremaine 1987), it is related to this resonance (Salo et al. 1999). Similarly the inner ring is related to the inner 4/1 resonance and the outer pseudoring to the outer Lindblad resonance. Some randomly chosen velocity vectors (in a coordinate system corotating with the bar) superimposed on the density distribution are shown in Fig. 1. The density distribution is represented on a logarithmic scale, because of the large density contrast between the nuclear ring and the outer disc.

The good fit of both the morphology and the velocity field (for detailed figures see Salo et al. 1999) suggest that our simple model is quite realistic. This also means that there is probably only one pattern speed present, with the possible exception of a nuclear bar.

3   THE DYNAMO CODE

We take a standard mean-field dynamo equation,

$$\frac{\partial \boldsymbol{B}}{\partial t} = \nabla \times (\boldsymbol{u} \times \boldsymbol{B} + \boldsymbol{u}_{\mathrm{dia}} \times \boldsymbol{B} + \alpha \boldsymbol{B} - \eta \nabla \times \boldsymbol{B}), \tag{1}$$

where, as usual, η is the turbulent magnetic diffusivity and α represents a conventional alpha effect. $\boldsymbol{u}$ comprises the large-scale velocities (circular and non-circular) and $\boldsymbol{u}_{\mathrm{dia}} = -\frac{1}{2}\nabla\eta$, and represents the turbulent diamagnetism (Vainshtein & Zeldovich 1972; Roberts & Soward 1975). In general we allow $\alpha = \alpha(\boldsymbol{r})$, $\eta = \eta(\boldsymbol{r})$, although in most of the models considered $\eta = $ constant (and so the diamagnetic term in equation 1 vanishes). Equation (1) is solved as an initial-value problem. In the computations discussed below, the initial conditions were usually that the initial ('seed') field was a mixture of axisymmetric and bisymmetric parts, with an energy significantly less than the equipartion value. However solutions are relatively insensitive to the initial conditions after a few rotation galactic periods (say 0.5 Gyr). We write $\eta = \eta_0\tilde{\eta}(\boldsymbol{r})$, $\boldsymbol{v} = v_0\tilde{\boldsymbol{v}}(\boldsymbol{r})$, with η_0 and v_0 being typical values of η and $|\boldsymbol{v}|$ respectively. We introduce a basic alpha-quenching mechanism by writing $\alpha = \alpha_0\tilde{\alpha}(\boldsymbol{r})f(\boldsymbol{B})$, where α_0 is a typical value of α and

$$f(\boldsymbol{B}) = \frac{1}{(1 + \alpha_B \boldsymbol{B}(\boldsymbol{r})^2/B_0^2)}, \tag{2}$$

where B_0 is the field strength in equipartition with the kinetic energy of the turbulent gas motions. α_B is a factor of order unity that will depend on details (unknown) of the alpha-quenching mechanism. Putting $\alpha_B = 0$ thus gives a linear calculation, and $\alpha_B \neq 0$ gives a non-linear calculation, with field strengths limited at about $B_0\alpha_B^{-1/2}$, or somewhat larger, especially in the presence of strong velocity

shear (cf. Moss et al. 1998b). We allow for the possibility of a spatial variation in the magnetic field–gas equilibrium condition caused by the the gas density and turbulent velocity varying with position, by writing $B_0 = \tilde{B}_0 b(r)$, where $\tilde{B}_0$ is a constant (see Sections 4 and 5.3).

If a sufficiently strong magnetic field affects the turbulent motions so as to reduce the alpha effect, it is possible that it also affects the turbulent resistivity η ('η-quenching'). However it is arguable that this effect is significantly smaller, as the alpha effect depends on the vorticity of the turbulence, whereas the turbulent diffusivity depends on its overall magnitude. Furthermore, there is no generally agreed or employed parametrization of η-quenching (but see Rüdiger & Kitchatinov 1993), and so its introduction would lead to further uncertainities. Thus we neglect this effect in the models described below.

We make the conventional assumption that $\eta \approx \frac{1}{3} u_t l_t$, where u_t and l_t are typical values of the velocity- and length-scales of the turbulence. In the Milky Way, near the disc plane, $u_t \sim 10$ km s^{-1}, $l_t \sim 100$ pc, giving an estimate for η of about 10^{26} cm^2 s^{-1}. However, conditions in barred galaxies such as IC 4214 may be rather different, and the above expression for η can only be regarded as an order-of-magnitude estimate. When η is a function of position, we define η_0 to be equal to or slightly greater than the maximum value of η. However, in most of the calculations that we discuss, η is a constant, equal to η_0. We can define the corresponding magnetic Reynolds numbers $R_\alpha = \alpha_0 L/\eta_0$, $Rm = v_0 L/\eta_0$, where L is a convenient length-scale: here we take $L = h$, a measure of the disc thickness. We define $v_0 = 1$ km s^{-1}, and choose α_0 such that the maximum value of α is approximately 1–5 km s^{-1}. R_m and the other conventional dynamo number, $R_\omega = \Omega_0 L^2/\eta_0$, are fixed exactly by the dynamo model parameters. [If $\Omega(r)$ is measured in units of km s^{-1} kpc^{-1}, then $\Omega_0 = 1$ km s^{-1} kpc^{-1}.] Lengths are scaled with R, the disc radius, and the unit of time is $T = L^2/\eta_0$. In relation (2), we set $\alpha_B = 1$ and $\tilde{B}_0 = 1$, so we are effectively scaling the field strength in units of $\tilde{B}_0 \alpha_B^{-1/2}$.

We note that for mean field theory to be valid, the scale of variation of the mean field should be greater than that of the small-scale field, which is approximately that of the turbulent motions. The interstellar turbulence is believed to have a typical scale of about 100 pc, so that provided the computed field has a scale of a few hundred pc or more, the treatment will be valid.
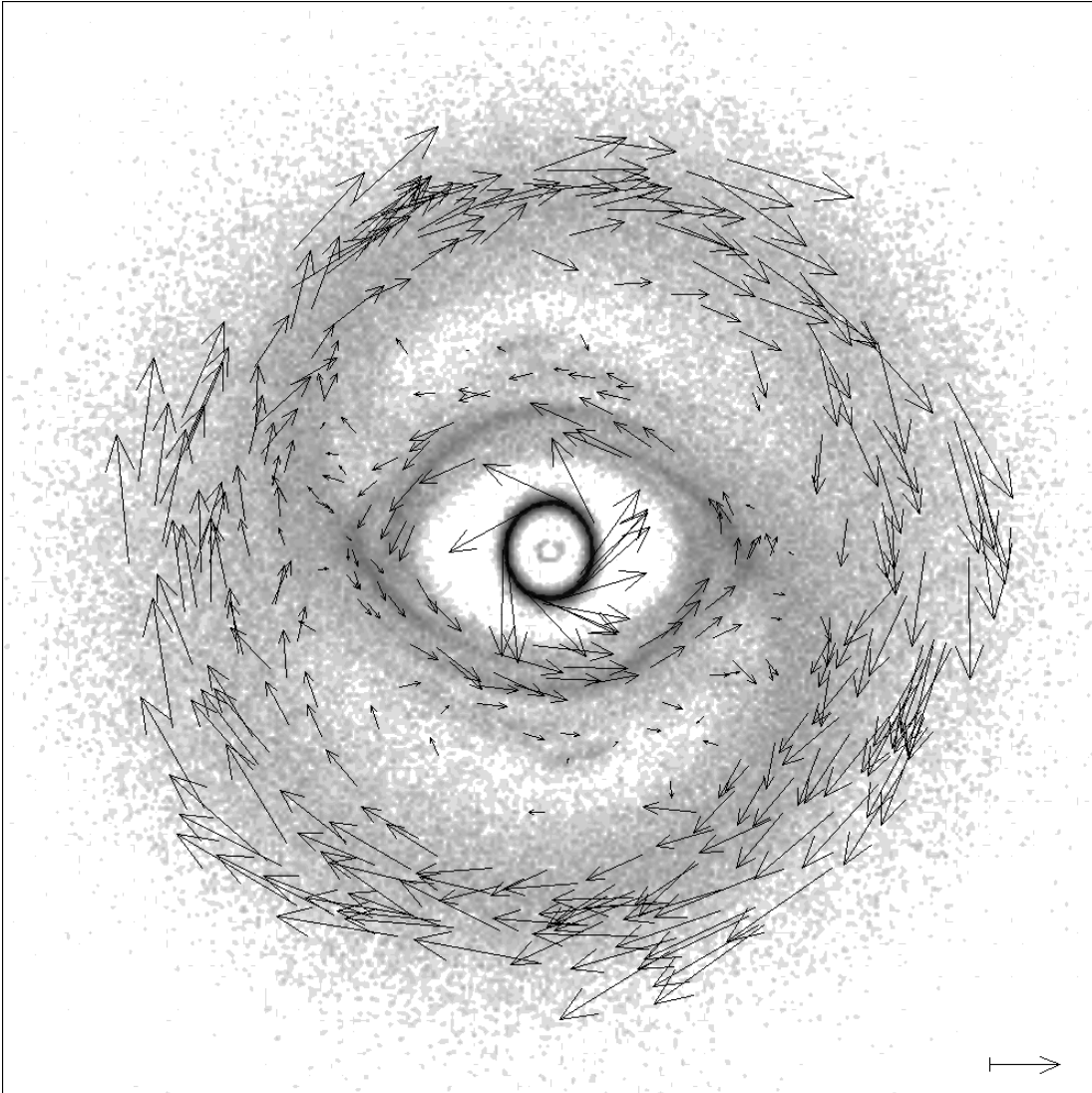

Figure 1. Gas velocity vectors for model I, superimposed on the density distribution, in the corotating frame. The scale vector in the lower left corner has a length of 150 km s^{-1}. The density is on a logarithmic scale, with the darkest shades showing the areas of highest density. The figure represents a region 30×30 kpc^2.

We use the two-dimensional 'no-z' (NZ) approximation, which is based on the idea of replacing z-derivatives by terms $\sim O(h^{-1})$, where h is the disc thickness or scaleheight (e.g. Subramanian & Mestel 1993; Moss 1995), and the code is in the form implemented in Moss et al. (1998a, see also Moss 1995), solving a modified version of equation (1) on $0 \le r \le R$, $0 \le \phi \le 2\pi$, with $NI \times NJ$ grid points and uniform meshing. For most of the computations we took $NI = NJ = 101$. Some were repeated with $NI = NJ = 201$, with little change. Note that Moss et al. (1998a) showed that the gross field structure obtained with a three-dimensional code, when projected on to the plane $z = 0$, was quite similar to that found with the NZ approximation.

With this approximation, magnetic fields are restricted to be of even (quadrupolar) parity with respect to the disc plane. Given that both theory and observation seem to predict that such fields are generally to be expected, we feel this is not a fundamental restriction at this stage of development of the theory.

In the majority of the work described here, we take η to be uniform, i.e. $\tilde{\eta} = 1$ and, for most of the computations, $\tilde{\alpha} = 1$ also. Boundary conditions are that $B_r = B_\phi = 0$ at $r = R$. Results were little affected for other plausible choices of boundary condition, provided that R was large enough for the dynamo-active region to be included well within the computational domain. $R = 15$ kpc was found to be a satisfactory choice. We take $h = 300$ pc (roughly equal to the vertical scalelength in the dynamical model), but previous experience (e.g. Moss et al. 1998a) suggests that results are insensitive to this choice.

4 REDUCTION OF VELOCITY AND DENSITY DATA

Velocity data is supplied by the dynamical simulation of Section 2 as (v_x, v_y) pairs at $O(10^5)$ points (x, y). These points correspond to the position of the fluid 'particles', and are correspondingly extremely non-uniformly distributed. The data was reduced as described as 'Method 1' in section 4.1 of Moss et al. (1998a). This technique of generating extra (Lagrangian) data points by combining velocity data from several equivalent times substantially reduces problems caused by 'holes' in the data, encountered in Moss et al. (1998a).
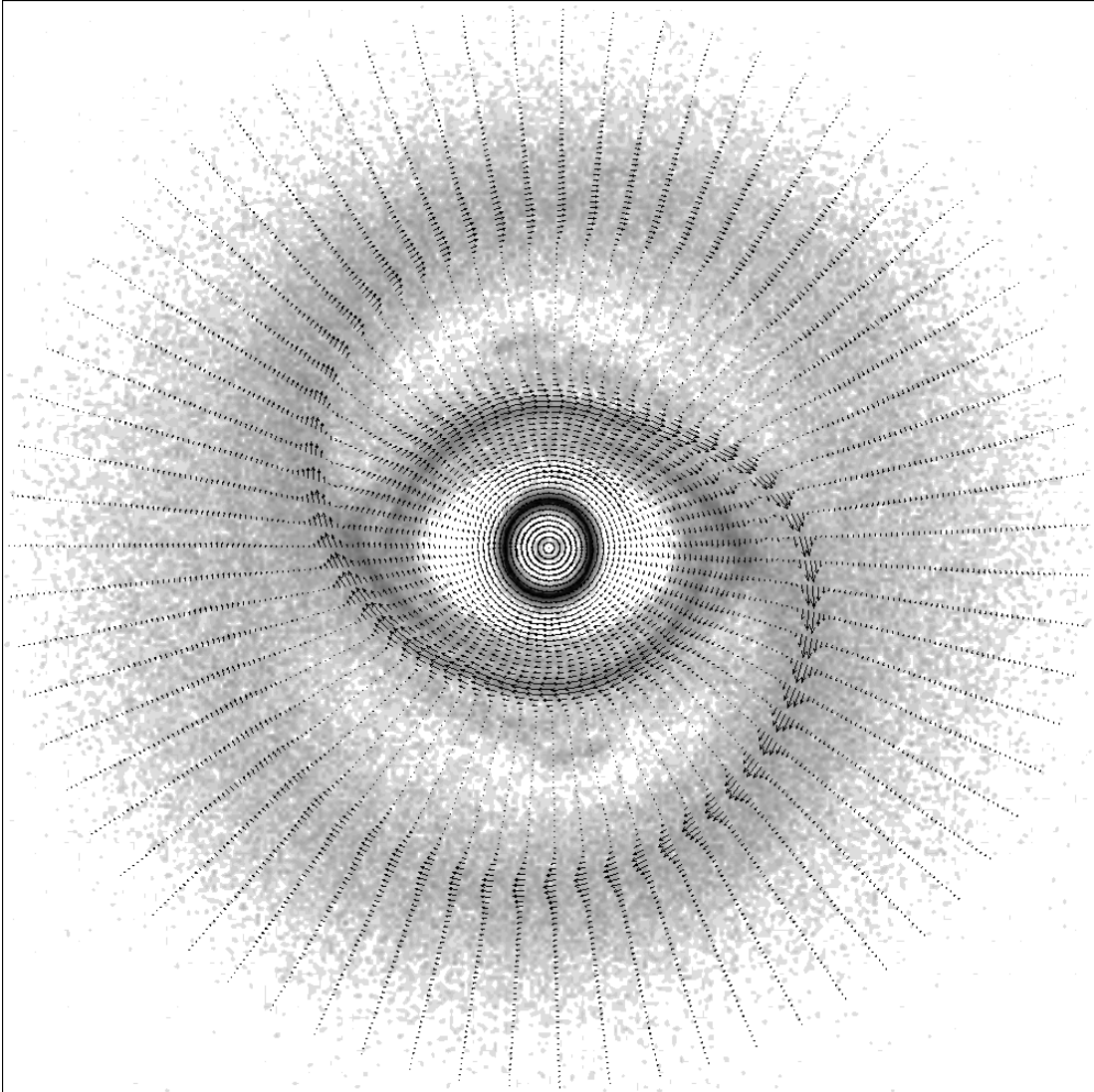

Figure 2. Magnetic field vectors for the standard dynamo calculation, using Model I, superimposed on the gas density distribution (logarithmic grey-scale). The figure has dimensions 30×30 kpc^2.

We also analysed the dynamical simulation data to produce a rotating density field $\rho(r, \omega_P t - \phi)$, where ω_P is the pattern speed. The density was naively estimated by counting the number of gas 'particles' per unit volume. In order to avoid very large fluctuations, caused partly by the patchiness inherent in the Lagrangian nature of the data,, we arbitrarily introduced a lower limit on the density of $\rho_0 = 0.01\rho_{max}$, where ρ_{max} is the largest value found.

5 RESULTS

5.1 The basic model

We took as standard a model with uniform resistivity $\eta = 2 \times 10^{26}$ cm^2 s^{-1}, uniform alpha coefficient $\alpha \approx 1$ km s^{-1}, and uniform equipartition field strength B_0 [i.e. $b(r) = 1$, Section 3]. The initial field is a combination of parts with azimuthal dependence $\exp(im\phi)$, with $m = 0$ and 1, varying on radial scale R. Using the velocity field of Model I (Section 2), we found that after several rotation periods the field structure is almost steady in a reference frame rotating with the pattern speed. In Fig. 2 we give a plot of the magnetic field vectors, superimposed on the density distribution, and in Fig. 3 we show the evolution with time of the energies in azimuthal Fourier modes $m = 0, 1, 2, 3$.

In this model corotation occurs at a radius about 10 per cent greater than the semi-major axis of the bar, i.e. at fractional radius $x_c = r/R \approx 0.4$. This is close to, but a little outside of, the radius at which the distinct magnetic arms emerge from the central regions.

As is apparent from the magnetic field plot of Fig. 2, large field gradients are present. This means that significant energy is present in the Fourier modes with larger m values. We show in Fig. 4 the azimuthal variation of selected field components at a typical time.

Limited experimentation showed that our results are insensitive to choice of initial field configuration. The exception is that the presence of an initial $m = 1$ field component gives a significant $m = 1$ component of magnetic field that persists for one or two Gyr (e.g. Fig. 3), plausibly supported by a parametric resonance mechanism of the sort described by Moss (1996). However, the energy in the $m = 1$ part of the field is always less that that in the $m = 2$ component, and the overall appearance of the field is little altered by the presence or absence of this contribution.

5.2 The role of the corotation radius

We also performed several numerical experiments in which the pattern speed of the frame in which the velocities were steady was artificially altered. These experiments were performed solely to determine the effects on the magnetic field structure of changing the corotation radius – it is not suggested that the resulting velocity fields are consistent dynamically, nor that they provide a good model for IC 4214. We show in Fig. 5 the resulting, almost steady, magnetic field pattern corotating with a pattern speed decreased by 25 per cent from the standard value of 37.3 km s^{-1} kpc^{-1} to 28 km s^{-1} kpc^{-1}. It is apparent from comparison of Fig. 5 with Fig. 2 that the radius at which the magnetic arms emerge has moved outwards, and this is typical of the several experiments performed. Eventually, as r_c approaches and then exceeds R, there is no marked steady corotating field pattern, and the non-axisymmetric field components (especially modes $m = 1, 3, \ldots$) decline steadily. In Table 1 we list the pattern speed, corotation radius and an estimate of the radius at which the magnetic arms begin for these experiments.

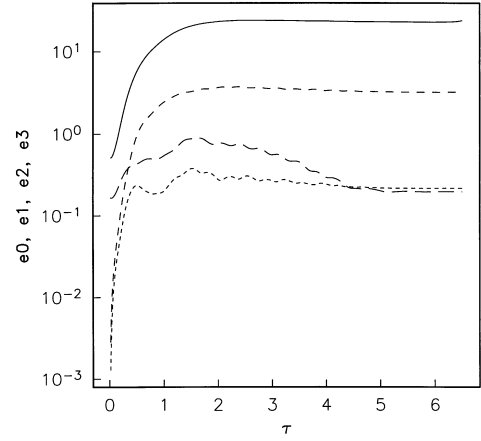The significance of the corotation radius is discussed in Section 6.

Figure 3. Evolution with time of energies in the azimuthal modes $m = 0, 1, 2, 3$ (respectively continuous, long-, medium- and short-dashed curves) for the calculation shown in Figs 1 and 2. The unit of time is 3.6×10^8 yr and the energy units are arbitrary.
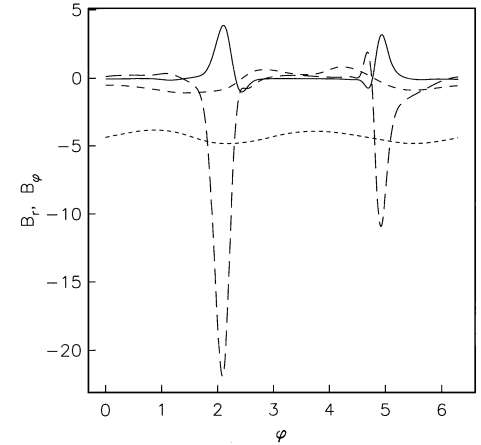

Figure 4. Variation with azimuthal angle ϕ of B_r, B_ϕ, at fractional radius $r/R = 0.5$, and of B_ϕ at $r/R = 0.1$ and 0.9 (respectively the solid, long-, medium- and short-dashed curves), for the model shown in Figs 1–3 (time about 1 Gyr from the start of the calculation).

Table 1. Summary of results when the pattern speed is artificially altered. ω_P is the pattern speed in km s^{-1} kpc^{-1}, r_c and r_A are the corotation radius and an estimate of the radius at which the arms begin, in kpc. The second entry, for $\omega_P = 37.3$ km s^{-1} kpc^{-1}, is for the basic model. The entry * indicates that there are no well-defined magnetic arms of the kind discussed in the text.

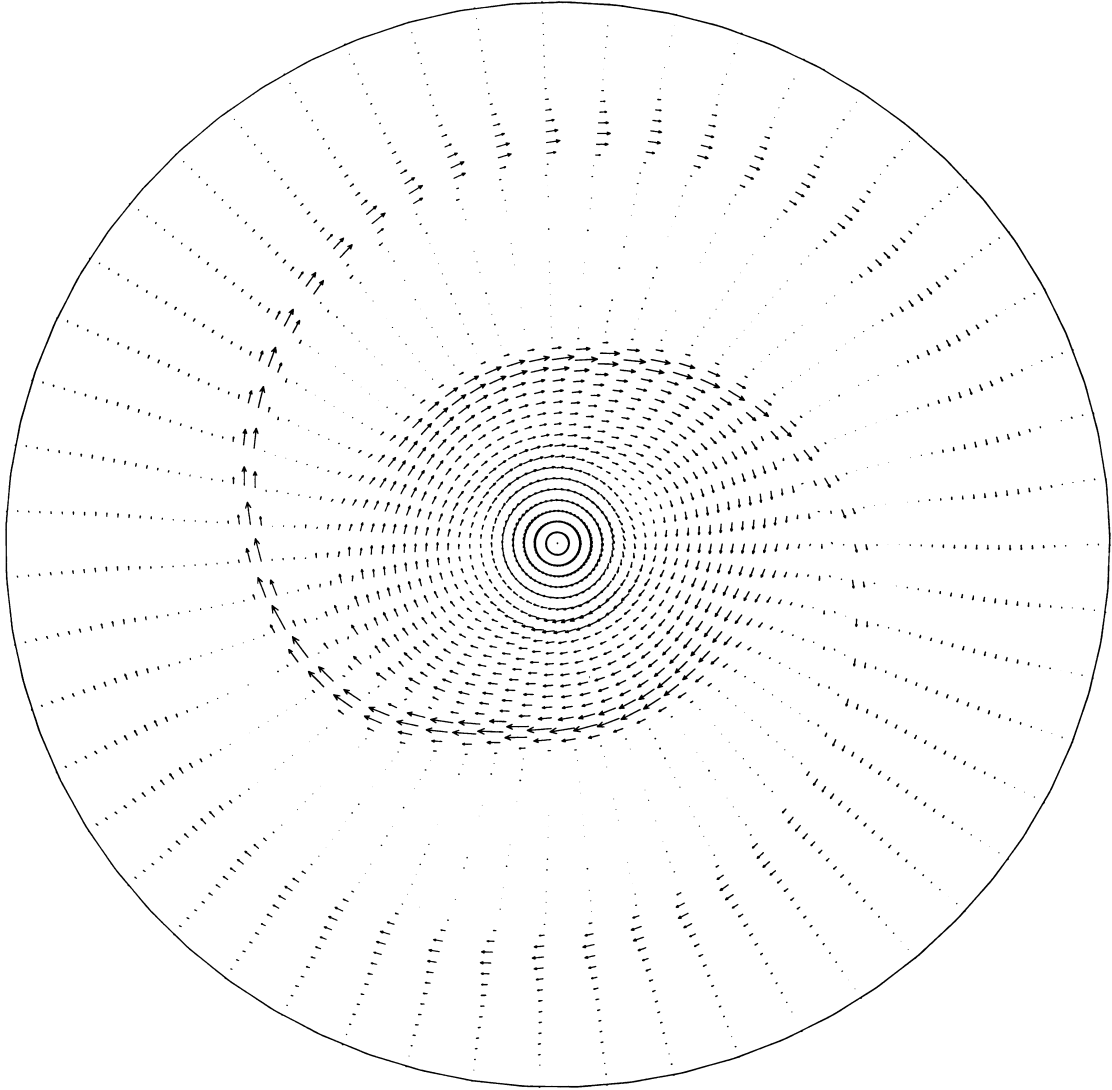| ω_P	r_c	r_A
56.0	4.4	2.6
37.3	6.0	4.8
28.0	7.5	6.4
18.6	10.0	7.4
9.3	15.3	*

Figure 5. Magnetic field vectors for the model with reduced pattern speed, $\omega_P = 28$ km s^{-1} kpc^{-1}.

5.3 Variations on the basic model

We experimented further by allowing the equipartition field strength B_0 to vary with position, $B_0^2 \propto \rho v_t^2$, where v_t is the turbulent velocity. As we have no information about v_t, we assumed it to be constant, but allowed ρ to vary as described in Section 4. A little surprisingly perhaps, the overall results appeared little affected. On reflection, this is probably because the strongest variation in ρ occurs in the central regions, where the non-axisymmetric field structure is relatively weak.

We also ran a calculation with a variable diffusion coefficient, $\eta = \eta(r)$. Here we were motivated by the theoretical and observational evidence that v_t is larger in spiral arms than in the interarm regions (e.g. Roberts & Hausmann 1984; Rohlfs & Kreitschmann 1987; Garciá-Burillo, Combes & Gerin 1993). If l_t, the turbulent length-scale, does not decrease, this implies an increase in $\eta \sim v_t l_t$. In order to investigate very crudely the importance of this effect, we took $\eta \propto 1 + \epsilon_\eta \sqrt{\rho/\rho_0}$, where ρ_0 is the reference density defined in Section 4. In this expression, ρ only appears as a proxy to indicate the position of gaseous structures, and thus for increased values of v_t, and so η. With ϵ_η chosen to give a ratio of maximum to minimum values of η of between 2 and 4, there was little overall change to the

results presented above for the basic model. In particular, the conspicuous magnetic arms were present. The main effect was that the non-axisymmetric field was stronger relative to the axisymmetric one near to the galactic centre, but the field was still predominantly axisymmetric in this region. We did not attempt to disentangle the competing effects of turbulent diamagnetism and the locally enhanced diffusion in this case. Naively, the advection of field by the term $\boldsymbol{u}_{\text{dia}} = -\frac{1}{2}\nabla\eta$ might be expected to concentrate the field in the arms, in opposition to the effects of the larger value of η, but almost certainly this interpretation is too simple.

5.4 A model with no inner Linblad resonance

As discussed in Section 2, the basic model (I) has an inner Linblad resonance, giving rise to the inner gas ring (see Fig. 1), situated within the bar region. In order to assess the importance of this feature, we ran a dynamo calculation with the velocity field determined by a quite similar dynamical simulation that did not possess this inner Linblad resonance (Model II, Section 2). The corotation radius for this model was at fractional radius $r/R \approx 0.3$. Here, as in the model of Section 5.1, α and η are uniform, with $\eta = 2 \times 10^{26}$ cm^2 s^{-1}. The resulting magnetic field structure is shown in Fig. 6.
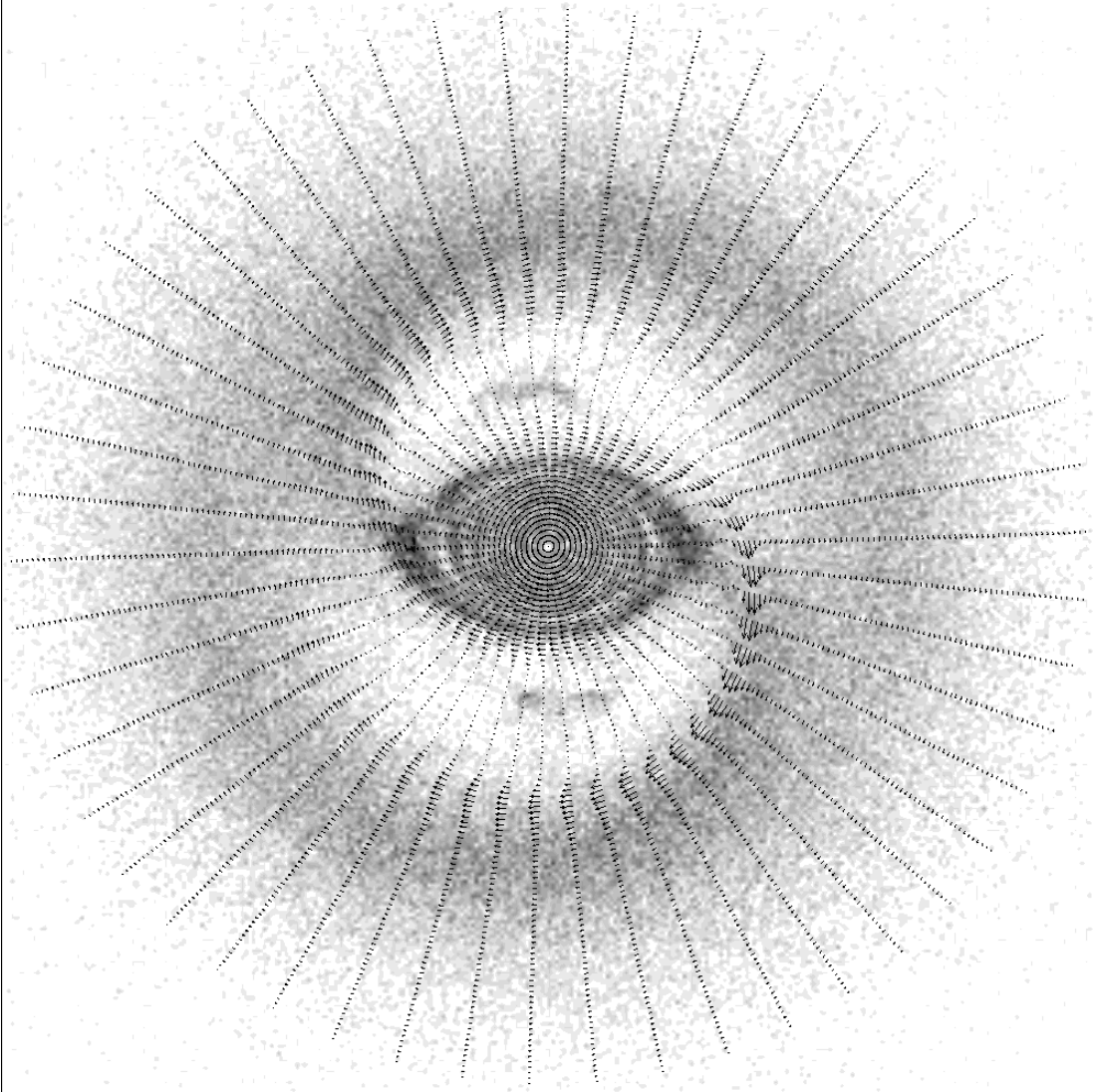
Figure 6. Magnetic field vectors for the calculation (model II) without an inner Linblad resonance, superimposed on the gas density distribution (logarithmic grey-scale). The figure has dimensions 30×30 kpc.[2]

6 DISCUSSION

Moss (1998) examined an idealized model of a galactic dynamo in which streaming occurred along spiral arms. This discussion was set in the context of a grand-design spiral galaxy, without a central bar, where streaming velocities of up to about 10 km s^{-1} might be expected. He showed that these motions could maintain significant non-axisymmetric magnetic fields over times greater than 10 or 20 mean galactic rotation periods by a mechanism connected with the location of the corotation radius, where the pattern speed and angular velocity of the gas coincide.

In these models, the underlying galactic dynamo produces an axisymmetric magnetic field. This is sheared by the non-circular velocities, to produce a non-axisymmetric field component. It is the radial shear that is significant here. Normally the non-axisymmetric part of the field is rapidly wound up by the differential rotation, resulting in a marked reduction of radial length-scales, and subsequent reconnection and dissipation. (This is essentially why non-axisymmetric fields are usually harder to excite than axisymmetric

ones, in a differentially rotating system.) However, when the streaming velocities rotate with the pattern speed, near the corotation radius, the winding up of field lines is much reduced and the non-axisymmetric field can continue to grow. The regions on the arms near corotation can act as a source of non-axisymmetric field, which is sheared azimuthally as it is advected, resulting in a large-scale spiral pattern. In contrast, experiments show that the same streaming velocities, if stationary in the *inertial* frame, produce a very much smaller non-axisymmetric magnetic field component, and a tightly wound field.

The former effect is what appears to be occurring in the current model for IC 4214. Here the $m = 0$ and $m = 2$ field components become very nearly steady, whereas the other Fourier components are much smaller and decrease in magnitude. The streaming velocities in these models are considerably larger than those assumed in Moss (1998). On the other hand the velocity field is not so 'clean' as the analytic form assumed there, but overall the effects seem stronger. The well-defined magnetic arms terminate at a relatively small distance inside the corotation radius. The

importance of this radius can be demonstrated by artificially changing the pattern speed input to the dynamo calculation. The radius at which the distinct arms terminate moves inwards and outwards with the corotation radius (see Table 1). Whilst this appears to provide a plausible explanation for the existence of long-lived magnetic arms, we agree that the coherence of the non-axisymmetric field structures over a relatively large extent in radius is perhaps a little surprising.

This mechanism can also be related to the parametric resonance associated with velocity streaming, discussed briefly in Moss (1996), especially when a $m = 1$ component is present in the initial field. However, the large magnitude of the non-circular velocities means that the field cannot be considered as a modification of any combination of basic non-axisymmetric modes calculated for an axisymmetric disc, but is clearly determined by the flow.

In Figs 2, 5 and 6 we have presented the magnetic fields resulting from velocity fields that differ in certain key properties (pattern speed, presence or absence of inner Linblad resonance). The overall magnetic patterns are quite similar, the most significant difference being the radius at which the magnetic arms emerge from the bar-dominated central region, which varies by the order of $0.1R$, i.e. $1-2$ kpc. Only if radio observations are of correspondingly high spatial resolution would these patterns be distinguishable observationally.

Moss (1996) discussed how 'contrast structures' – very steep azimuthal gradients of magnetic field – could arise in the presence of large-scale gas streaming. Fig. 4 suggests that this effect occurs here. Moreover, we find that if the computations are continued for times longer than about a couple of Gyr at our standard spatial resolution, a slow progression in the field gradients occurs, which eventually causes an instability in the numerical algorithm used to solve equation (1). (The associated change in the field structure is almost indiscernable.) The onset of this instability can be deferred by increasing the azimuthal resolution of the finite-difference grid, but for any given resolution it occurs eventually. This is very similar to the behaviour described in Moss (1996).

7   CONCLUSIONS

In this paper we believe that we have, for the first time, modelled a dynamo in a specific barred spiral galaxy, with a good representation of the large-scale velocity field, in particular the non-circular motions. In this galaxy, there does not appear to be a shock present in the bar (at least not to the resolution of the observed velocity field), and this feature has simplified the modelling somewhat. We note that such shocks are commonly present in these barred galaxies, and have important effects on both the magnetic and velocity fields (e.g. Frick et al. 1998). Nevertheless, in NGC 6946, another weakly barred system, studied by Frick et al., the observed large-scale field is approximately axisymmetric near the galactic centre (within the bar region), whereas non-axisymmetric field structures ('magnetic spiral arms') emerge from near the ends of the bar and extend to larger radii. These features are quite similar to those present in our magnetic field models.

Several papers have previously addressed some aspects of the general problem of the magnetic field structure present in barred spiral galaxies. As discussed in the Introduction, none of these addresses simultaneously all the factors that we have included. We have adopted the simplest mean field dynamo model to represent the effects of small-scale (turbulent) gas motions. The most striking feature of our results is the existence of coherent, long-lived magnetic arms, rotating with the pattern speed defined by the bar.

There is no evidence from our calculations that these structures will decay, given our assumption that the velocity field is unchanging. Aside from the particular interest of these results for our specific model, we feel that they are rather more general in nature. Given any galactic dynamo that preferentially produces an axisymmetric magnetic field in the absence of non-circular motions (the situation with many dynamo models), gas streaming that rotates with the pattern speed will excite a large-scale non-axisymmetric field structure, if the corotation radius is not close to the centre or outside of the galaxy. This condition seems likely to be satisfied in many barred spiral galaxies, where the corotation radius is near to the end of the bar. Thus, even if the crucial mechanism that converts toroidal magnetic field to poloidal in equation (1) is not the mean-field alpha effect, the salient points of our discussion, and the main result, will remain.

REFERENCES

Beck R., Brandenburg A., Moss D., Shukurov A., Sokoloff D., 1996, ARA&A, 34, 155
Binney J., Tremaine S., 1987, Galactic Dynamics. Princeton Univ. Press, Princeton NJ
Buta R., 1995, ApJS, 96, 39
Buta R., Purcell G. B., Lewis M., Crocker D. A., Salo H., Rautiainen P., 1999, AJ, in press
Byrd G., Rautiainen P., Salo H., Buta R., Crocker D. A., 1994, AJ, 108, 476
Chiba M., Lesch H., 1994, A&A, 284, 731
Combes F., 1996, in Buta R., Crocker D. A., Elmegreen B. G., eds, ASP Conf. Ser. 91, IAU Colloq. 157, Barred Galaxies. Astron. Soc. Pac., San Francisco, p. 286
Combes F., Gerin M., 1985, A&A, 150, 327
Frick P., Beck R., Shukurov A., Sokoloff D., Ehle M., Kamphuis J., 1998, MNRAS, submitted
Garciá-Burillo S., Combes F., Gerin M., 1993, A&A, 274, 148
Hunter J. H., Ball R., Huntley J. M., England M. N., Gottesman S. T., 1988, ApJ, 324, 721
Lindblad P. A. B., Lindblad P. O., Athannasoula E., 1996, A&A, 313, 65.
Moss D., 1995, MNRAS, 275, 191
Moss D., 1996, A&A, 315, 63
Moss D., 1998, MNRAS, 297, 860
Moss D., Korpi M., Rautiainen P., Salo H., 1998a, A&A, 329, 895
Moss D., Shukurov A., Sokoloff D. D., Berkhuijsen E. M., Beck R., 1998b, A&A, 335, 500
Moss D., Shukurov A., Sokoloff D., 1999, A&A, in press
Otmianowska-Mazur K., Chiba M., 1995, A&A, 301, 41
Otmianowska-Mazur K., von Linden S., Lesch H., Skupniewicz G., 1997, A&A, 323, 56
Parker E. N., 1992, ApJ, 401, 137
Roberts W. W., Hausmann M. A., 1984, ApJ, 277, 744
Roberts P. H., Soward A. M., 1975, Astron. Nachr., 296, 49
Rohlfs K., Kreitschmann J., 1987, A&A, 178, 95
Rüdiger G., Kitchatinov L. L., 1993, A&A, 269, 581
Salo H., 1991, A&A, 243, 118
Salo H., Rautiainen P., Buta R., Purcell G.B, Lewis M., Crocker D. A., Laurikainen E., 1999, AJ, in press
Schwarz M. P., 1981, ApJ, 247, 77
Subramanian K., Mestel L., 1993, MNRAS, 265, 649
Vainshtein S. I., Zeldovich, Ya. B., 1972, Sov. Phys. – Usp., 15, 159

This paper has been typeset from a T_EX/L^AT_EX file prepared by the author.